Pharmacologic activation of the G protein-coupled estrogen receptor inhibits pancreatic ductal adenocarcinoma

Christopher A. Natale[1,2], Jinyang Li[3], Tzvete Dentchev[1], Brian C. Capell[1], John T. Seykora[1], Ben Z. Stanger[3], and Todd W. Ridky[1]*

1. Perelman School of Medicine, Department of Dermatology, University of Pennsylvania, Philadelphia, PA 19104, USA
2. Linnaeus Therapeutics Inc., Philadelphia, Pennsylvania 19146, USA.
3. Perelman School of Medicine, Abramson Family Cancer Research Institute, University of Pennsylvania, Philadelphia, Pennsylvania 19104, USA.

Summary

In a previous paper (Natale et al., 2018) we showed that signaling through the G protein-coupled estrogen receptor (GPER) likely contributes to improved clinical outcomes in women with melanoma. Here we used murine syngeneic tumor models and human xenografts to test whether GPER signaling inhibits pancreatic ductal adenocarcinoma (PDAC). Activation of GPER with the specific, small molecule agonist G-1 inhibited PDAC proliferation, depleted c-Myc and programmed death ligand 1 (PD-L1), and increased tumor cell immunogenicity. Systemically delivered G-1 significantly lengthened survival, and increased the efficacy of immune therapy in PDAC bearing mice. We detected GPER protein in a majority of spontaneous human PDAC tumors. This finding, coupled with our previous melanoma data, and the wide tissue distribution of GPER, suggest that GPER agonists may be useful against many different cancer types.

Introduction

For many cancers, incidence and age-adjusted mortality rates are lower in females than in males, suggesting that biological differences between the sexes influence tumor initiation, progression, and response to modern therapeutics (1-3). Understanding the mechanisms responsible for these differences may lead to identification of new therapeutic targets for cancer, including malignancies that are not classically considered sex hormone responsive. Recently, we demonstrated that nonclassical estrogen signaling through the G protein-coupled estrogen receptor (GPER) drives melanocyte differentiation and inhibits melanoma (4, 5). In mice with therapy-resistant syngeneic melanoma, systemic administration of a specific small molecule GPER agonist, G-1 (6), induced differentiation in tumor cells that inhibited proliferation and rendered tumors more immunogenic. Combination therapy with G-1 and α-PD-1

immune-checkpoint blockade demonstrated combinatorial anti-tumor activity, with a high percentage of complete responses (50%) that were associated with long-lasting tumor immunity (4). GPER is expressed in many tissues (7) and signaling downstream of GPER is mediated by ubiquitous cellular proteins that mediate cAMP signaling. Therefore, we hypothesized that selective GPER activation would inhibit other cancers in addition to melanoma, and similarly potentiate the anti-tumor activity of α-PD-1 and other immunotherapies.

To test this idea, we turned to pancreatic ductal adenocarcinoma (PDAC), a highly aggressive cancer that is poorly responsive to current therapy, and a major cause of cancer death in the United States (8). As with many cancers, women have lower PDAC incidence and more favorable outcomes than men, suggesting that estrogen may suppress PDAC (1, 2, 9). Consistent with this, use of estradiol containing oral contraceptives, and history of multiple pregnancies (which necessarily correlates with high estrogen exposure) are both associated with decreased PDAC risk (10-12). Further supporting the idea that PDAC is influenced by estrogen are human clinical trials showing that tamoxifen, which is a GPER agonist, extends survival in PDAC patients (13, 14). These data, coupled with lack of clear evidence that nuclear estrogen receptors are expressed and functional in PDAC (15), led us to consider the possibility that estrogen may influence PDAC through GPER.

Li and colleagues recently generated a library of clonal PDAC tumor cell lines from a genetically engineered mouse model of PDAC, KPCY ('KPCY' mice, KRas $^{LSL\text{-}G12D/+}$; Trp53 $^{L/+}$ or Trp53 $^{LSL\text{-}R172H/+}$; Pdx1-Cre; Rosa- YFP), that faithfully recapitulates the molecular, histological, and clinical features of the human disease (16-18). In syngeneic, immunocompetent C57BL/6 mice, the degree of immune infiltration varies with each cell line. This variability reflects the natural heterogeneity in immune infiltrates observed in human PDAC. Here we used these new models to test whether GPER activation affects PDAC tumor growth, and/or improves response to immune checkpoint blockade.

Results and Discussion

To test whether PDAC responds to GPER signaling, we used three of the genetically defined murine PDAC tumor lines that together represent the heterogeneity in immune infiltration and response to immunotherapy: 6419c5 tumors attract minimal CD8+ T cell infiltration and respond poorly to

combination therapy with cytotoxic and immune activating agents, 2838c3 tumors attract robust CD8+ T cell infiltration and are highly responsive to therapy, and 6499c4 tumors which are associated with robust CD8+ T-cell infiltration, but only modest responses to therapy (18).

GPER is expressed in all 3 PDAC tumor lines at levels similar to YUMM1.7 melanoma (Figure 1A), which we previously showed is highly responsive to GPER signaling (4). To test whether the effects of GPER activation in PDAC paralleled those in melanoma, we treated the PDAC tumor cell lines with the specific GPER agonist G-1, and observed similar dose-dependent decreases in p-RB, c-Myc, and PD-L1. These changes were associated with decreased proliferation and a G_1-S cell cycle block (Figure 1B-J). As in melanoma, G-1 inhibited tumor cell proliferation without inducing cell death (Figure 1K).

To test the effects of selective GPER in PDAC cells in an unbiased way, we performed RNA-Seq and HALLMARK gene set enrichment analysis on 2838c3, 6419c5, 6499c4 tumor cells treated with G-1 vs. vehicle control (Figure 1L). Consistent with the protein and proliferative changes (Figure 1), GPER activation was associated with decreased expression of genes involved in cell proliferation, invasion, and immune evasion including: epithelial-to-mesenchymal transition drivers, E2F targets, c-Myc targets, and cell cycle checkpoint regulators. These data are all consistent with the hypothesis that GPER signaling is generally tumor suppressive.

We next tested whether G-1 might have therapeutic utility as a systemically delivered agent for established PDAC, with and without immune checkpoint inhibitors. Mice harboring syngeneic PDAC were treated with subcutaneous G-1, αPD-1 antibody, or both, and tumor growth and survival were compared to matched controls treated with vehicle and isotype antibody controls (Figure 2A-D). All three PDAC tumor models responded to G-1 monotherapy with rapid initial tumor regression and prolonged survival. Tumor response to αPD-1 was different in each tumor line, but was significantly potentiated by G-1 in 2 of the 3 lines. 2838c3 was highly responsive to both G-1 and αPD-1, and the combination of both agents completely cleared tumors in 60% of animals with no evidence of disease at day 100, suggesting a combinatorial benefit. 6419c5 responded to G-1 but was completely resistant to αPD-1 monotherapy. However, G-1 and αPD-1 combination therapy extended survival beyond G-1 monotherapy, again

suggesting combinatorial benefit. In contrast, combination therapy did not provide any additional benefit over G-1 monotherapy in 6499c4 tumors, which were only minimally responsive to αPD-1 alone.

In an effort to understand the mechanistic basis for the heterogeneous responses to the G-1 and αPD-1 combination regimen, we next tested whether PD-L1 is expressed in each tumor. Using *in situ* hybridization for PD-L1 in naïve tumors, we detected high levels of PD-L1 expression in 2838c3 and 6419c5, and complete absence of PD-L1 in 6499c4 (Figure 2E), suggesting that the combinatorial survival-promoting effect of G-1 and αPD-1 depends on whether the tumor cells express PD-L1.

Next, we used well-established human PDAC cell lines, harboring the activating K-Ras mutation that drives the vast majority of human PDAC, to test whether GPER activation has similar effects in human models. GPER is expressed in PANC-1, HPAC, and MIA PaCa-2 cells at levels comparable to GPER expression in WM46 melanoma (Figure 2-figure supplement 1A), which we previously showed was highly responsive to GPER activation (4). To test whether the effects of GPER signaling in human PDAC paralleled those in melanoma and murine PDAC, we treated the human PDAC tumor cell lines with G-1, and observed similar dose-dependent decreases in p-RB, and c-Myc, which were paralleled by decreases in proliferation (Figure 2-figure supplement 1B-G). We also observed decreased PD-L1 in HPAC and MIA PaCa-2 cells, but did not observe PD-L1 protein in untreated PANC-1 cells. To test whether G-1 has therapeutic utility against human PDAC in vivo, we treated nude mice harboring HPAC and MIA PaCa-2 tumors with subcutaneous G-1 one week after tumor implantation. (The PANC-1 cell line failed to establish tumors in nude mice following our protocol.) Treatment with G-1 significantly inhibited tumor growth and prolonged survival relative to vehicle treated controls (Figure 2-figure supplement 2H-K). As these studies with human PDAC models were conducted in immunodeficient mice, it was not possible to test for combinatorial activity with immune therapy, as we did in the murine models. Nonetheless, these in vitro and in vivo data using human PDAC are consistent with our findings in mouse models, and together support the idea that GPER activation with G-1 inhibits PDAC.

We next questioned whether GPER was expressed in spontaneous human PDAC. Using a tissue microarray representing several stages of PDAC, immunohistochemical staining for GPER demonstrated both peripheral membrane and punctate cytoplasmic staining, alone or in combination in tumor cells.

There was a wide range of staining intensity across different clinical stages (Figure 3A-B). Overall, GPER was detected in 61% of the PDAC cases tested, suggesting that GPER may be a widely expressed, and pharmacologically accessible therapeutic target in human PDAC.

Together with our previous study on melanoma, this work raises the possibility that GPER agonists may have therapeutic utility against a wide array of GPER-expressing cancer types, and critically, may extend the utility of modern immune therapeutics to tumors, such as PDAC, that have thus far been resistant to immune therapy (19). These data highlight the importance of G protein-coupled receptor signaling in cancer, demonstrate that activation of GPER is tumor suppressive in cancers that are not classically hormone responsive, and indicate that GPER activity may contribute to biological differences between the sexes that influence cancer progression and response to modern therapies.

Figure Legends

Figure 1. *GPER activation inhibits PDAC*. (**A**) GPER western blot of lysates from murine YUMM1.7 melanoma cells and murine PDAC cells. (**B**) Western analysis of lysates from 2838c3 PDAC cells treated for 16 hours with increasing concentrations of G-1. (**C**) Proliferation of 2838c3 PDAC cells treated with 250nM G-1, n=5 per group, * denotes significance by two-way ANOVA. (**D**) Cell cycle analysis of 2838c3 PDAC cells treated with 250nM G-1, n=3 per group. (**E**) Western analysis of lysates from 6419c5 PDAC cells treated for 16 hours with increasing concentrations of G-1. (**F**) Proliferation of 6419c5 PDAC cells treated with 250nM G-1, n=5 per group, * denotes significance by two-way ANOVA. (**G**) Cell cycle analysis of 6419c5 PDAC cells treated with 250nM G-1, n=3 per group. (**H**) Western analysis of lysates from 6499c4 PDAC cells treated for 16 hours with increasing concentrations of G-1. (**I**) Proliferation of 6499c4 PDAC cells treated with 250nM G-1, n=5 per group, * denotes significance by two-way ANOVA. (**J**) Cell cycle analysis of 6499c5 PDAC cells treated with 250nM G-1, n=3 per group. (**K**) Viability assay of murine PDAC cells treated with 250nM G-1, n=3 per group. (**L**) MSigDB HALLMARK gene set enrichment analysis of overlapping upregulated and downregulated genes in 2838c3, 6419c5, and 6499c4 cells treated with 250nM G-1 for 16 hours.

Figure 2. *The specific GPER agonist G-1 inhibits murine PDAC in vivo.* (**A**) Experimental timeline of murine PDAC-bearing mice treated with subcutaneously delivered vehicle or 10mg/kg G-1, as well as 10mg/kg αPD-1 antibody or isotype antibody control (2A3), n=5 per group. (**B**) Tumor volumes of 2838c3 PDAC tumors one day after the final treatment with 10mg/kg G-1, n=10 per group, * denotes significance by one-way ANOVA. (**C**) 2838c3 tumor volumes measured over time; line terminates after first survival event in the group, n=5 per group. (**D**) Survival curve of 28383-bearing mice treated with vehicle or 10mg/kg G-1, as well as 10mg/kg αPD-1 antibody or 10mg/kg isotype antibody control (2A3), significance between groups by the Log-Rank (Mantel-Cox) test is listed in the table below. (**E**) Tumor volumes of 6419c5 PDAC tumors one day after the final treatment with 10mg/kg G-1, n=10 per group, * denotes significance by one-way ANOVA. (**F**) 6419c5 tumor volumes measured over time; line terminates after first survival event in the group, n=5 per group. (**G**) Survival curve of 6419c5-bearing mice treated with vehicle or 10mg/kg G-1, as well as 10mg/kg αPD-1 antibody or 10mg/kg isotype antibody control (2A3), significance between groups by the Log-Rank (Mantel-Cox) test is listed in the table below. (**H**) Tumor volumes of 6499c4 PDAC tumors one day after the final treatment with 10mg/kg G-1, n=10 per group, * denotes significance by one-way ANOVA. (**I**) 6499c4 tumor volumes measured over time; line terminates after first survival event in the group, n=5 per group. (**J**) Survival curve of 6499c4-bearing mice treated with vehicle or 10mg/kg G-1, as well as 10mg/kg αPD-1 antibody or 10mg/kg isotype antibody control (2A3), significance between groups by the Log-Rank (Mantel-Cox) test is listed in the table below. (**K**) in situ hybridization for PD-L1 in murine PDAC tumors, 40x magnification, scale bar=50um.

Figure 2-figure supplement 1. *The specific GPER agonist G-1 inhibits human PDAC.* (**A**) GPER western blot of lysates from human WM46 melanoma cells and human PDAC cells. (**B**) Western analysis of lysates from PANC-1 PDAC cells treated for 16 hours with increasing concentrations of G-1. (**C**) Proliferation of PANC1 PDAC cells treated with 500nM G-1, n=5 per group, * denotes significance by two-way ANOVA. (**D**) Western analysis of lysates from HPAC PDAC cells treated for 16 hours with increasing concentrations of G-1. (**E**) Proliferation of HPAC PDAC cells treated with 500nM G-1, n=5 per group, * denotes significance by two-way ANOVA. (**F**) Western analysis of lysates from MIA PaCa-2 PDAC cells treated for 16 hours with increasing concentrations of G-1. (**G**) Proliferation of MIA PaCa-2 PDAC cells treated with 500nM G-1, n=5 per group, * denotes significance by two-way ANOVA. (**H**) HPAC tumor volumes measured over time; line terminates after first survival event in the group, n=5 per group. (**I**) Survival curve of HPAC-bearing mice treated with vehicle or 10mg/kg G-1 on day 7-9, 14-16, and 21-23 (3 weekly pulses), significance between groups by the Log-Rank (Mantel-Cox) test. (**J**) MIA PaCa-2 tumor volumes measured over time; line terminates after first survival event in the group, n=5 per group. (**K**) Survival curve of MIA PaCa-2-bearing mice treated with vehicle or 10mg/kg G-1 on day 7-9, 14-16, and 21-23 (3 weekly pulses), significance between groups by the Log-Rank (Mantel-Cox) test.

Figure 3. *GPER is expressed in human PDAC clinical samples*. (**A**) Representative images of normal human pancreas and stage 1A-IV PDAC stained for GPER, 40x magnification, scale bar=50um. (**B**) Pathologist scoring of the pancreatic tissue microarray stained for GPER, scoring index was determined by scoring the percentage of positive cells on a scale of 0 to 3, as well as the intensity of GPER staining on a scale of 0 to 3, these scores were multiplied to generate the scoring index.

Figure 1

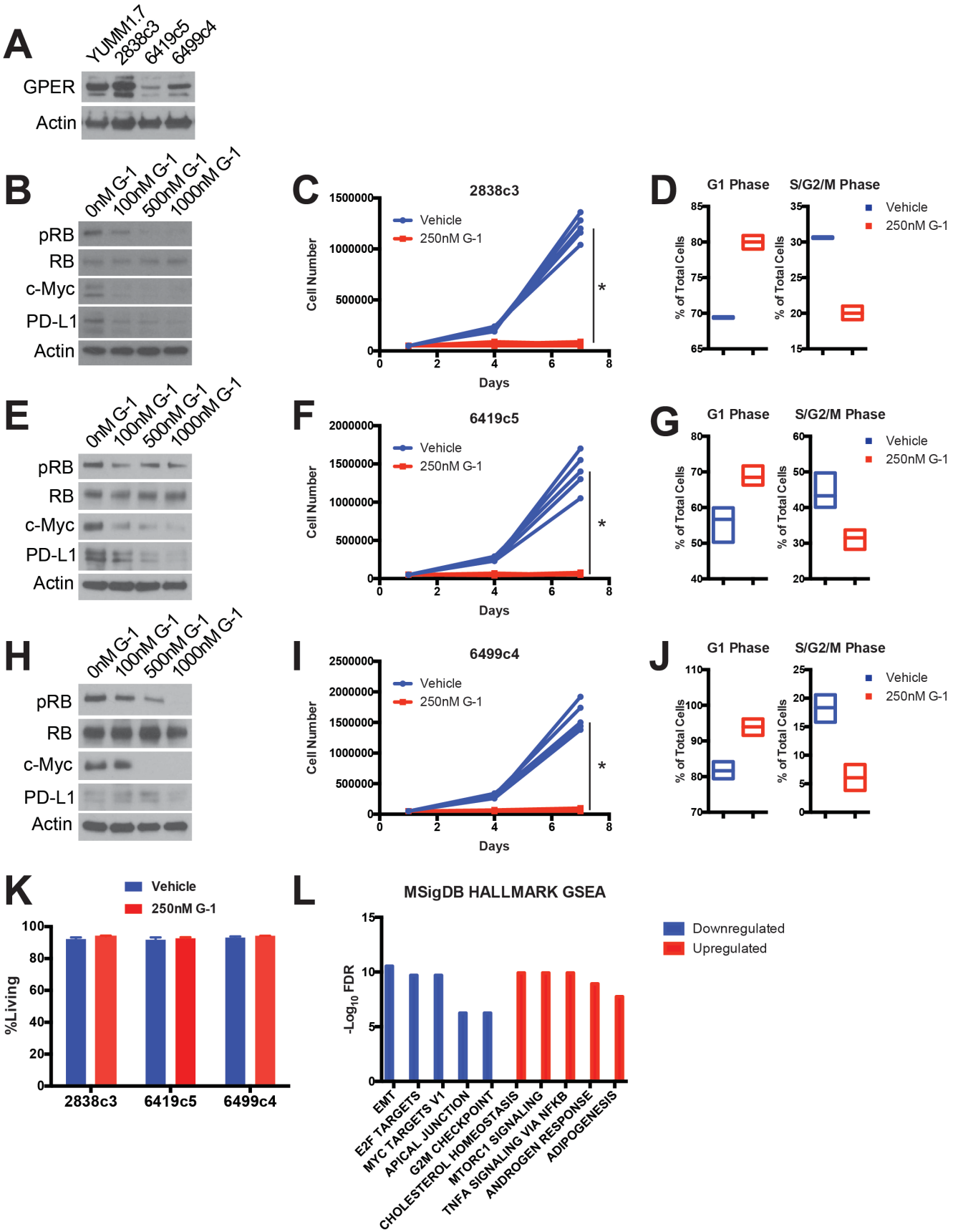

Figure 2

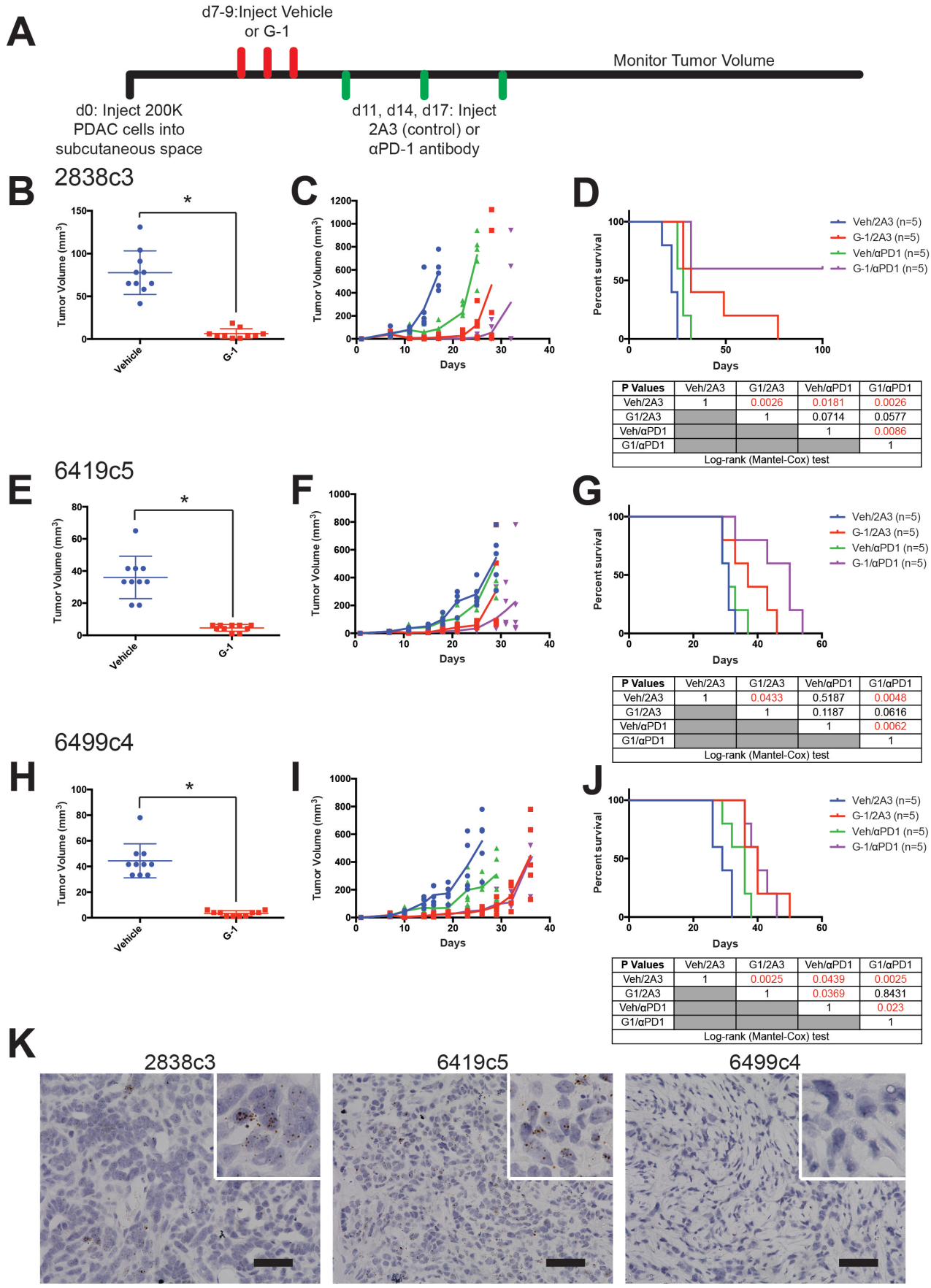

P Values	Veh/2A3	G1/2A3	Veh/αPD1	G1/αPD1
Veh/2A3	1	0.0026	0.0181	0.0026
G1/2A3		1	0.0714	0.0577
Veh/αPD1			1	0.0086
G1/αPD1				1
Log-rank (Mantel-Cox) test				

P Values	Veh/2A3	G1/2A3	Veh/αPD1	G1/αPD1
Veh/2A3	1	0.0433	0.5187	0.0048
G1/2A3		1	0.1187	0.0616
Veh/αPD1			1	0.0062
G1/αPD1				1
Log-rank (Mantel-Cox) test				

P Values	Veh/2A3	G1/2A3	Veh/αPD1	G1/αPD1
Veh/2A3	1	0.0025	0.0439	0.0025
G1/2A3		1	0.0369	0.8431
Veh/αPD1			1	0.023
G1/αPD1				1
Log-rank (Mantel-Cox) test				

Figure 2: Figure Supplement 1

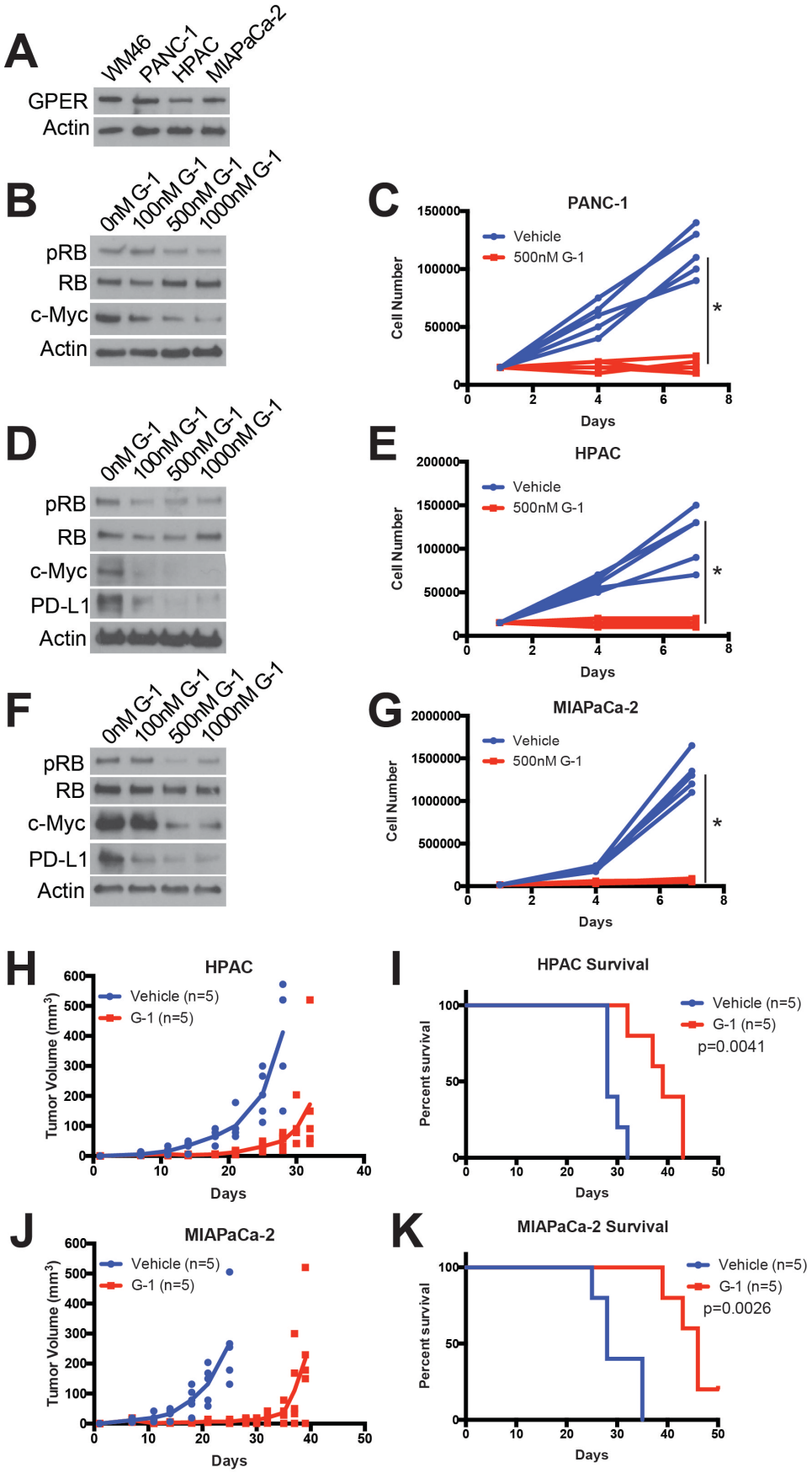

Figure 3

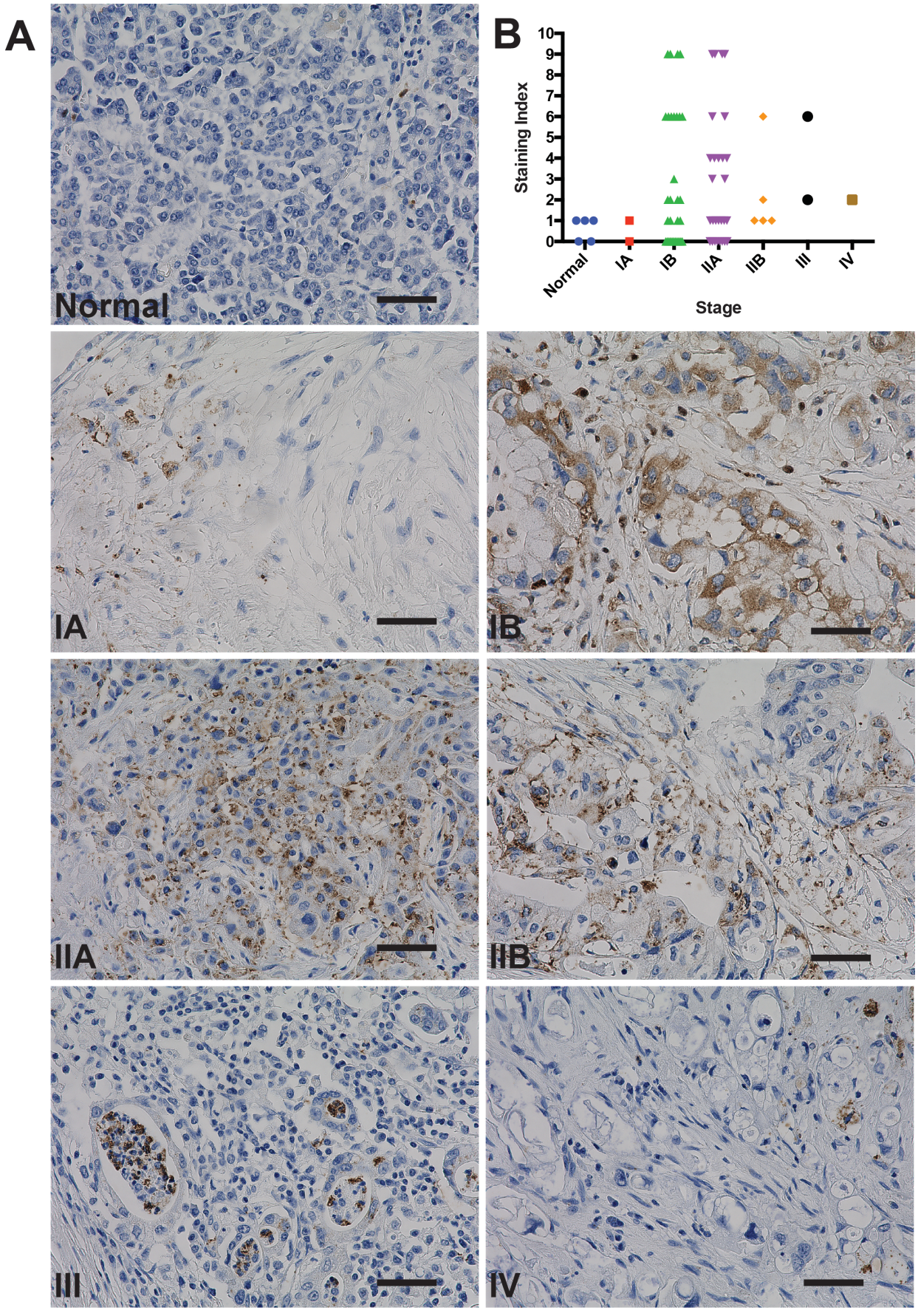

Methods

Cell culture and cell lines

2838c3, 6419c5, 6499c4 murine PDAC cells were derived in the laboratory of Ben Stanger (University of Pennsylvania) and cultured in DMEM (Mediatech, Manassas, VA, USA) with 5% FBS (Invitrogen, Carlsbad, CA, USA) and 1% antibiotic-antimycotic (Invitrogen). PANC-1, HPAC, and MIA PaCa-2 cell lines were a gift from the laboratory of Ben Stanger (University of Pennsylvania) and cultured in DMEM (Mediatech) with 5% FBS (Invitrogen) and 1% antibiotic-antimycotic (Invitrogen). WM46 melanoma cells were a gift from Meenhard Herlyn (Wistar Institute, Philadelphia, PA, USA) and were cultured in TU2% media. Tumor cells were regularly tested using MycoAlert Mycoplasma Detection Kit from Lonza (Allendale, NJ, USA). G-1 (10008933) was purchased from Cayman Chemical (Ann Arbor, MI, USA). Cells were trypsinized using 0.05% Trypsin with EDTA (Invitrogen) for 5 minutes to detach from the plate.

Mice

All mice were purchased from Jackson Laboratories (Bar Harbor, ME, USA). Five to seven week old female C57BL/6J or nude (NU/J) mice were allowed to acclimatize for one week prior to being used for experiments. These studies were preformed without inclusion/exclusion criteria or blinding, but included randomization. Based on a twofold-anticipated effect, we performed experiments with at least 5 biological replicates. All procedures were performed in accordance with International Animal Care and Use Committee (IACUC)-approved protocols at the University of Pennsylvania.

Subcutaneous tumors and treatments

Subcutaneous tumors were initiated by injecting tumor cells in 50% Matrigel (Corning, Bedford, MA, USA) into the subcutaneous space on the left and right flanks of mice. 2×10^5 of murine PDAC cells or 5×10^5 human PDAC cells were used for each tumor. In vivo G-1 treatments were performed by first dissolving G-1, synthesized as described previously (5), in 100% ethanol at a concentration of 1mg/ml. The desired amount of G-1 was then mixed with an appropriate volume of sesame oil, and the ethanol was evaporated off using a Savant Speed Vac (Thermo Fisher Scientific, Waltham, MA, USA), leaving the desired amount of G-1 dissolved in 50μL of sesame oil per injection at a 10mg/kg dose. Vehicle injections were prepared in an identical manner using 100% ethanol. Vehicle and G-1 injections were delivered through subcutaneous injection as indicated in each experimental timeline. Isotype control antibody (Clone: 2A3, BioXcell, West Lebanon, NH, USA) and αPD-1 antibody (Clone: RMP1-14, BioXcell) were diluted in sterile PBS and delivered through intraperitoneal injections at a dose of 10mg/kg.

Survival Analysis

As subcutaneous tumors grew in mice, perpendicular tumor diameters were measured using calipers. Volume was calculated using the formula L × W^2 × 0.52, where L is the longest dimension and W is the perpendicular dimension. Animals were euthanized when tumors exceeded a protocol-specified size of 15 mm in the longest dimension. Secondary endpoints include severe ulceration, death, and any other condition that falls within the IACUC guidelines for Rodent Tumor and Cancer Models at the University of Pennsylvania.

Western Blot Analysis

Adherent cells were washed once with DPBS, and lysed with 8M urea containing 50mM NaCl and 50mM Tris-HCl, pH 8.3, 10mM dithiothreitol, 50mM iodoacetamide. Lysates were quantified (Bradford assay), normalized, reduced, and resolved by SDS gel electrophoresis on 4–15% Tris/Glycine gels (Bio-Rad, Hercules, CA, USA). Resolved protein was transferred to PVDF membranes (Millipore, Billerica, MA, USA) using a Semi-Dry Transfer Cell (Bio-Rad), blocked in 5% BSA in TBS-T and probed with primary antibodies recognizing β-Actin (Cell Signaling Technology, #3700, 1:4000, Danvers, MA, USA), c-Myc (Cell Signaling Technology, #13987, 1:1000), GPER (Sigma, HPA027052, 1:500), HLA-ABC (Biolegend, w6/32,1:500, San Diego, CA, USA), human PD-L1 (Cell Signaling Technology, #13684, 1:1000), mouse PD-L1 (R&D systems, AF1019, 1:500, Minneapolis, MN, USA), p-RB (Cell Signaling Technology, #8516,

1:1000), and RB (Cell Signaling Technology, #9313, 1:1000). After incubation with the appropriate secondary antibody, proteins were detected using either Luminata Crescendo Western HRP Substrate (Millipore) or ECL Western Blotting Analysis System (GE Healthcare, Bensalem, PA). All western blots were repeated at least 3 times.

Immunohistochemistry and Quantification

FFPE tissue microarrays were purchased from Biomax (9461e, Derwood, MD, USA) and were stained GPER (Novus Biologics, NLS1183, Littleton, CO, USA) as previously described with some modifications (4). Briefly, slides have been deparaffinized and rehydrated in extend time than standard immunohistochemistry protocol (in three xylenes 7 min each time, 3 times 100% alcohol, 2 time 95% alcohol, ones 70% and 50% alcohol and finished with distill water). The antigen retrieval was done by immersing the slides in Tris-EDTA pH 8.0 and microwave for 14 minutes at power 9 then cool down to room temperature on the bench, washed three times in wash buffer and blocked sequentially the endogenous peroxidase and non-specific protein binding. The volume and the dilution/concentration (500 ul per slide at the dilution 1:70) of the primary antibody was calculate considering the total area of tissue and incubate overnight at 40C . Following multiple washes secondary antibody, goat anti-rabbit conjugated to HRP was applied, incubated for 20 minutes at room temperature, then washed out and signal was amplified with substrate-DAB chromogen buffer. The tissues were counterstain with hematoxylin, dehydrated, cover-slipped and analyzed. A board-certified pathologist performed scoring of the stained tissue microarray, and scoring index was determined by scoring the percentage of positive cells on a scale of 0 to 3 as well as the intensity of GPER staining on a scale of 0 to 3, these scores were multiplied to generate the scoring index value.

Cell cycle analysis

Tumor cells were cultured in 10% FBS in DMEM following standard cell culture protocol. Hoechst 33342 (ThermoFisher Scientific, #H1399) was added directly to the cell culture medium with the final concentration of 10 ug/mL 1 hour before sample collection. Cells were incubated with Hoechst 33342 at 37C for 1 hour. Then, cells were prepared to single cell suspension using trypsin and washed with PBS twice. Cells were resuspended in flow buffer (1% FBS in PBS) for flow analysis in a BD LSR II flow cytometry machine. Flow results were analyzed using the FlowJo software to assess the percentage of cells in G1 phase and S-G2-M phase.

Cell viability analysis

Tumor cells were cultured in 10% FBS in DMEM following standard cell culture protocol. Cells were prepared to single cell suspension using trypsin and washed with PBS twice. Cells were resuspended in flow buffer (1% FBS in PBS) with DAPI (ThermoFisher Scientific, #D21490) incubation for flow analysis in a BD LSR II flow cytometry machine. Flow results were analyzed using the FlowJo software to assess the percentage of cells with negative staining of DAPI.

RNA-seq

RNA was extracted using RNeasy kit (Qiagen catalog no. 74014) following the manufacturer's instructions. All RNA-seq libraries were prepared using the NEBNext Poly(A) mRNA Magnetic Isolation Module followed by NEBNext Ultra Directional RNA Library Prep Kit for Illumina (both from NEB). Library quality was analyzed using Agilent BioAnalyzer 2100 (Agilent) and libraries were quantified using NEB Library Quantification Kits (NEB). Libraries were then sequenced using a NextSeq500 platform (75bp, single-end reads) (Illumina). All RNA-seq was aligned using RNA STAR under default settings to Homo sapiens UCSC hg19 (RefSeq & Gencode gene annotations). FPKM generation and differential expression analysis was performed using DESeq2. DESeq2 output was analyzed by comparing differentially expressed genes with $p<0.05$ and HALLMARK gene set enrichment analysis was performed using MSigDB database (20).

RNA in situ hybridization analysis

Tumor cells were subcutaneously implanted into C57BL/6 mice for tumor growth. Tumors were collected 3 weeks after implantation, fixed with Zinc Formalin Fixative (Polysciences, #21516), and embedded in paraffin. Tumor sample paraffin sections were used for RNA in situ hybridization analysis using the RNAscope 2.5 HD Assay – BROWN (Advanced Cell Diagnosis) with probe targeting CD274 (PD-L1) (420501). The RNA in situ hybridization analysis was performed following standard procedures from the kit manual and published protocol (21) (RNAscope: a novel in situ RNA analysis platform for formalin-fixed, paraffin-embedded tissues).

Statistical Analysis

All statistical analysis was performed using Graphpad Prism 8 (Graphpad Software, La Jolla, CA, USA). No statistical methods were used to predetermine sample size. Details of each statistical test used are included in the figure legends.

Acknowledgements

The authors thank the University of Pennsylvania Skin Biology and Disease Research-based center for analysis of tissue sections. The authors also thank Michael Feigin, Miriam Doepner, and Junqian Zhang for critical pre-submission review. T.W.R. is supported by a grant from the NIH/NCI (R01 CA163566), a Penn/Wistar Institute N.I.H. SPORE (P50CA174523), the Melanoma Research Foundation, and the Dermatology Foundation. C.A.N was supported by an NIH/NIAMS training grant (T32 AR0007465-32) and an NIH/NCI F31 NRSA Individual Fellowship (F31 CA206325). This work was supported in part by the Penn Skin Biology and Diseases Resource-based Center (P30-AR069589). This work was also supported in part by a phase I STTR from the NIH/NCI (R41CA228695). The contents are solely the responsibility of the authors and do not necessarily represent the official views of the NIH.

Ethics Statement

This study was performed in strict accordance with the recommendations in the Guide for the Care and Use of Laboratory Animals of the National Institutes of Health. All of the animals were handled according to approved institutional animal care and use committee (IACUC) protocol (#803381) of the University of Pennsylvania.

Competing Interests

C.A.N. is listed as an inventor on a patent application held by the University of Pennsylvania related to this work (PCT/US2017/035278) and is a cofounder and current employee of the Penn Center for Innovation supported startup Linnaeus Therapeutics Inc. T.W.R. is listed as an inventor on a patent application (PCT/US2017/035278) held by the University of Pennsylvania related to this work, and is a cofounder and consultant to the Penn Center for Innovation supported startup Linnaeus Therapeutics Inc.

The authors have no additional financial interests.

References

1. Cook MB, Dawsey SM, Freedman ND, Inskip PD, Wichner SM, Quraishi SM, Devesa SS, McGlynn KA. Sex disparities in cancer incidence by period and age. Cancer Epidemiol Biomarkers Prev. 2009;18(4):1174-82. doi: 10.1158/1055-9965.EPI-08-1118. PubMed PMID: 19293308; PMCID: PMC2793271.
2. Cook MB, McGlynn KA, Devesa SS, Freedman ND, Anderson WF. Sex disparities in cancer mortality and survival. Cancer Epidemiol Biomarkers Prev. 2011;20(8):1629-37. doi: 10.1158/1055-9965.EPI-11-0246. PubMed PMID: 21750167; PMCID: PMC3153584.
3. McQuade JL, Daniel CR, Hess KR, Mak C, Wang DY, Rai RR, Park JJ, Haydu LE, Spencer C, Wongchenko M, Lane S, Lee DY, Kaper M, McKean M, Beckermann KE, Rubinstein SM, Rooney I, Musib L, Budha N, Hsu J, Nowicki TS, Avila A, Haas T, Puligandla M, Lee S, Fang S, Wargo JA, Gershenwald JE, Lee JE, Hwu P, Chapman PB, Sosman JA, Schadendorf D, Grob JJ, Flaherty KT, Walker D, Yan Y, McKenna E, Legos JJ, Carlino MS, Ribas A, Kirkwood JM, Long GV, Johnson DB, Menzies AM, Davies MA. Association of body-mass index and outcomes in patients with metastatic melanoma treated with targeted therapy, immunotherapy, or chemotherapy: a retrospective, multicohort analysis. Lancet Oncol. 2018. doi: 10.1016/S1470-2045(18)30078-0. PubMed PMID: 29449192.
4. Natale CA, Li J, Zhang J, Dahal A, Dentchev T, Stanger BZ, Ridky TW. Activation of G protein-coupled estrogen receptor signaling inhibits melanoma and improves response to immune checkpoint blockade. Elife. 2018;7. doi: 10.7554/eLife.31770. PubMed PMID: 29336307; PMCID: PMC5770157.
5. Natale CA, Duperret EK, Zhang J, Sadeghi R, Dahal A, O'Brien KT, Cookson R, Winkler JD, Ridky TW. Sex steroids regulate skin pigmentation through nonclassical membrane-bound receptors. Elife. 2016;5. doi: 10.7554/eLife.15104. PubMed PMID: 27115344; PMCID: PMC4863824.
6. Bologa CG, Revankar CM, Young SM, Edwards BS, Arterburn JB, Kiselyov AS, Parker MA, Tkachenko SE, Savchuck NP, Sklar LA, Oprea TI, Prossnitz ER. Virtual and biomolecular screening converge on a selective agonist for GPR30. Nature chemical biology. 2006;2(4):207-12. doi: 10.1038/nchembio775. PubMed PMID: 16520733.
7. Olde B, Leeb-Lundberg LM. GPR30/GPER1: searching for a role in estrogen physiology. Trends Endocrinol Metab. 2009;20(8):409-16. doi: 10.1016/j.tem.2009.04.006. PubMed PMID: 19734054.
8. Rahib L, Smith BD, Aizenberg R, Rosenzweig AB, Fleshman JM, Matrisian LM. Projecting cancer incidence and deaths to 2030: the unexpected burden of thyroid, liver, and pancreas cancers in the United States. Cancer research. 2014;74(11):2913-21. doi: 10.1158/0008-5472.CAN-14-0155. PubMed PMID: 24840647.
9. Ma J, Siegel R, Jemal A. Pancreatic cancer death rates by race among US men and women, 1970-2009. J Natl Cancer Inst. 2013;105(22):1694-700. doi: 10.1093/jnci/djt292. PubMed PMID: 24203988.
10. Zhu B, Zou L, Han J, Chen W, Shen N, Zhong R, Li J, Chen X, Liu C, Shi Y, Miao X. Parity and pancreatic cancer risk: evidence from a meta-analysis of twenty epidemiologic studies. Sci Rep. 2014;4:5313. doi: 10.1038/srep05313. PubMed PMID: 24936955; PMCID: PMC4060503.
11. Lee E, Horn-Ross PL, Rull RP, Neuhausen SL, Anton-Culver H, Ursin G, Henderson KD, Bernstein L. Reproductive factors, exogenous hormones, and pancreatic cancer risk in the CTS. Am J Epidemiol. 2013;178(9):1403-13. doi: 10.1093/aje/kwt154. PubMed PMID: 24008905; PMCID: PMC3813312.

12. Andersson G, Borgquist S, Jirstrom K. Hormonal factors and pancreatic cancer risk in women: The Malmo Diet and Cancer Study. Int J Cancer. 2018;143(1):52-62. doi: 10.1002/ijc.31302. PubMed PMID: 29424426; PMCID: PMC5969235.
13. Wong A, Chan A. Survival benefit of tamoxifen therapy in adenocarcinoma of pancreas. A case-control study. Cancer. 1993;71(7):2200-3. PubMed PMID: 8384066.
14. Theve NO, Pousette A, Carlstrom K. Adenocarcinoma of the pancreas--a hormone sensitive tumor? A preliminary report on Nolvadex treatment. Clin Oncol. 1983;9(3):193-7. PubMed PMID: 6616993.
15. Satake M, Sawai H, Go VL, Satake K, Reber HA, Hines OJ, Eibl G. Estrogen receptors in pancreatic tumors. Pancreas. 2006;33(2):119-27. doi: 10.1097/01.mpa.0000226893.09194.ec. PubMed PMID: 16868476.
16. Hingorani SR, Wang L, Multani AS, Combs C, Deramaudt TB, Hruban RH, Rustgi AK, Chang S, Tuveson DA. Trp53R172H and KrasG12D cooperate to promote chromosomal instability and widely metastatic pancreatic ductal adenocarcinoma in mice. Cancer Cell. 2005;7(5):469-83. doi: 10.1016/j.ccr.2005.04.023. PubMed PMID: 15894267.
17. Rhim AD, Mirek ET, Aiello NM, Maitra A, Bailey JM, McAllister F, Reichert M, Beatty GL, Rustgi AK, Vonderheide RH, Leach SD, Stanger BZ. EMT and dissemination precede pancreatic tumor formation. Cell. 2012;148(1-2):349-61. doi: 10.1016/j.cell.2011.11.025. PubMed PMID: 22265420; PMCID: PMC3266542.
18. Li J, Byrne KT, Yan F, Yamazoe T, Chen Z, Baslan T, Richman LP, Lin JH, Sun YH, Rech AJ, Balli D, Hay CA, Sela Y, Merrell AJ, Liudahl SM, Gordon N, Norgard RJ, Yuan S, Yu S, Chao T, Ye S, Eisinger-Mathason TSK, Faryabi RB, Tobias JW, Lowe SW, Coussens LM, Wherry EJ, Vonderheide RH, Stanger BZ. Tumor Cell-Intrinsic Factors Underlie Heterogeneity of Immune Cell Infiltration and Response to Immunotherapy. Immunity. 2018. doi: 10.1016/j.immuni.2018.06.006. PubMed PMID: 29958801.
19. Morrison AH, Byrne KT, Vonderheide RH. Immunotherapy and Prevention of Pancreatic Cancer. Trends Cancer. 2018;4(6):418-28. doi: 10.1016/j.trecan.2018.04.001. PubMed PMID: 29860986.
20. Subramanian A, Tamayo P, Mootha VK, Mukherjee S, Ebert BL, Gillette MA, Paulovich A, Pomeroy SL, Golub TR, Lander ES, Mesirov JP. Gene set enrichment analysis: a knowledge-based approach for interpreting genome-wide expression profiles. Proceedings of the National Academy of Sciences of the United States of America. 2005;102(43):15545-50. doi: 10.1073/pnas.0506580102. PubMed PMID: 16199517; PMCID: PMC1239896.
21. Wang F, Flanagan J, Su N, Wang LC, Bui S, Nielson A, Wu X, Vo HT, Ma XJ, Luo Y. RNAscope: a novel in situ RNA analysis platform for formalin-fixed, paraffin-embedded tissues. J Mol Diagn. 2012;14(1):22-9. doi: 10.1016/j.jmoldx.2011.08.002. PubMed PMID: 22166544; PMCID: PMC3338343.